AIP | Applied Physics Letters

Fast chirality reversal of the magnetic vortex by electric current

W. L. Lim, R. H. Liu, T. Tyliszczak, S. G. Erokhin, D. Berkov, and S. Urazhdin

Citation: Applied Physics Letters **105**, 222405 (2014); doi: 10.1063/1.4902997
View online: http://dx.doi.org/10.1063/1.4902997
View Table of Contents: http://scitation.aip.org/content/aip/journal/apl/105/22?ver=pdfcov
Published by the AIP Publishing

Fast chirality reversal of the magnetic vortex by electric current

W. L. Lim,[1,a)] R. H. Liu,[1] T. Tyliszczak,[2] S. G. Erokhin,[3] D. Berkov,[4] and S. Urazhdin[1,b)]
[1]*Department of Physics, Emory University, Atlanta, Georgia 30322, USA*
[2]*Advanced Light Source, Lawrence Berkeley National Laboratory, Berkeley, California 94720, USA*
[3]*Innovent Technology Development, Pruessingstr. 27B, Jena D-07745, Germany*
[4]*General Numerics Research Lab e.V., An der Leite 3b, Jena D-07749, Germany*

(Received 16 September 2014; accepted 18 November 2014; published online 1 December 2014)

The possibility of high-density information encoding in magnetic materials by topologically stable inhomogeneous magnetization configurations such as domain walls, skyrmions, and vortices has motivated intense research into mechanisms enabling their control and detection. While the uniform magnetization states can be efficiently controlled by electric current using magnetic multilayer structures, this approach has proven much more difficult to implement for inhomogeneous states. Here, we report direct observation of fast reversal of magnetic vortex by electric current in a simple planar structure based on a bilayer of spin Hall material Pt with a single microscopic ferromagnetic disk contacted by asymmetric electrodes. The reversal is enabled by a combination of the chiral Oersted field and spin current generated by the nonuniform current distribution in Pt. Our results provide a route for the efficient control of inhomogeneous magnetization configurations by electric current. © *2014 AIP Publishing LLC*. [http://dx.doi.org/10.1063/1.4902997]

The development of miniaturized magnetic devices[1,2] has been enabled by the possibility to directly manipulate the uniform magnetization state by electric current due to the transfer of angular momentum (or spin) from one ("fixed") magnetic layer to another ("free") layer.[3,4] However, this mechanism is generally inefficient for nonuniform magnetization states due to the reduced efficiency of spin transfer and difficulty in imparting the desired configuration both on the fixed and the free layers.[5]

Fast and efficient magnetization reversal by current has been demonstrated for uniformly magnetized structures.[6–8] However, control of nonuniform magnetization states, such as domain walls,[9] skyrmions,[10] and magnetization vortices,[11] by electric current has proven more challenging,[12,13] because of the difficulty in imparting the desired configuration both on the fixed and the free layers, as well as reduced efficiency of spin transfer in nonuniform configurations. The interest in these nonuniform configurations is motivated by their topological stability, making them insensitive to small perturbations and permitting closely packed arrays to be implemented for high density information storage.[14–21]

Here, we demonstrate the possibility to efficiently reverse the chirality of the magnetic vortex by current in a simple planar device based on a bilayer of Pt with a permalloy (Py) magnetic disk. The operation of our device is facilitated by the asymmetric Cu electrodes attached to the Py/Pt disk (Fig. 1(a)). The device structure consisted of a bilayer of a 8 nm thick Pt and 7 nm thick $Ni_{80}Fe_{20}$ = Py patterned into a disk with diameter of 820 nm, with two 100 nm thick Cu electrodes deposited on top. One of the electrodes forms a sharp point at the center of the disk, while the other forms a semi-circular contact around the rim. When a voltage is applied between the electrodes, current flows radially through the disk (red arrows in Fig. 1(a)), producing two effects that enable vortex reversal. First, the spin Hall effect in Pt[22,23] generates a spin current with a chiral distribution of spins. The resulting spin torque (ST) exerted on the magnetization of Py due to the outward current flow stabilizes the clockwise vortex state, as viewed from top in Fig. 1(b), and destabilizes the counterclockwise state. Conversely, inward radial current stabilizes the counterclockwise and destabilizes the clockwise vortex state, resulting in the reversal of chirality when the current is reversed. In addition to ST, radial current produces an Oersted field with the same chiral symmetry as the magnetic vortex (green circular arrow in Fig. 1(b)). In our device configuration, both of these contributions stabilize the same chirality of the vortex state.

The reversal was detected by two complementary techniques. The first technique relied on a combination of anisotropic magnetoresistance of Py and the chirality-dependent response of the vortex state to external field. As illustrated in the top view schematic of Fig. 2(b), the core of the counterclockwise vortex is displaced to the left (right) by the upward (downward) field, and vice versa for the clockwise vortex. When the vortex core is displaced from the disk center to the

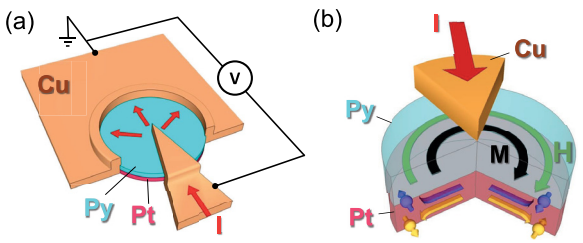

FIG. 1. Device geometry and the effects of the applied current. (a) Schematic of the device: current *I* flows from a triangular Cu electrode into a Pt/Py bilayer disk and spreads radially (red arrows) towards a semicircular Cu electrode. (b) Spin current flows towards the Py disk due to the spin Hall effect in Pt. The distribution of spins (yellow and violet arrows) is circulating around the disk following the current distribution. The black semicircular arrow shows the magnetization configuration of the vortex, and the green arrow qualitatively shows the distribution of the Oersted field of the current.

a)wlimnd@gmail.com
b)sergei.urazhdin@emory.edu

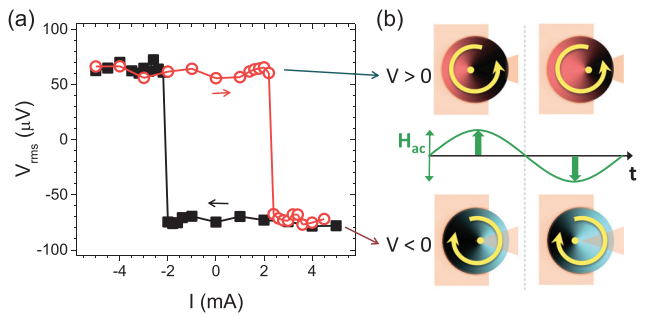

FIG. 2. Electronic detection of vortex reversal with an *ac* magnetic field. (a) Voltage V for a Pt/Py disk measured at in-plane *ac* field $H_{ac} = 7$ Oe applied perpendicular to increasing current I (red circles) and decreasing I (black squares), showing hysteretic voltage jumps at critical currents $I = \pm 2$ mA corresponding to the reversal of the magnetic vortex. The voltages are induced by the changes in anisotropic magnetoresistance of the disk due to the displacement of the vortex core caused by H_{ac}. (b) Schematics of the time-dependent magnetization configurations at $V > 0$ (upper panels, red vortex with anticlockwise chirality) and $V < 0$ (lower panels, blue vortex with clockwise chirality) at peak values (thick green arrows) of $H_{ac}(t)$ (green curve). Positive and negative signs of V correspond to two magnetic vortex states with opposite chiralities (yellow circular arrows): for anti-clockwise chirality, the *ac* voltage response follows in phase with H_{ac}, while for clockwise chirality, the phase of the response is opposite to that of H_{ac}. Yellow dots indicate the position of the vortex core.

left in the schematic of Fig. 2(b), the Py magnetization becomes, on average, closer to the direction of the current flow, resulting in a larger resistance due to the anisotropic magnetoresistance of Py. Conversely, displacement of the core to the right lowers the resistance. By applying a small in-plane ac magnetic field and a dc current to the device, we can induce an oscillation of vortex core, and consequently the voltage across the device will be in- and out-of-phase with the ac field depending on the vortex chirality. The hysteresis loop in Fig. 2(a) was obtained by applying the values of current I marked on the horizontal axis, then reducing the dc current to a small value of 0.1 mA. The ac voltage between the electrodes induced by the vortex oscillations is plotted on the vertical axis. The voltage exhibits hysteretic switching to a positive (in-phase with ac field) value at $I < -2$ mA and negative (out-of-phase) value at $I > 2$ mA, Fig. 2(a). These results demonstrate the possibility to directly control the vortex chirality by applying a modest electric current of appropriate sign.[24]

To confirm our interpretation of electronic measurements, we performed direct time-resolved imaging of the current-dependent magnetic configuration using x-ray magnetic circular dichroism (XMCD) microscopy.[25,26] A sequence of current pulses with opposite polarities was applied to the device (top panel in Fig. 3(a)). Insets in Fig. 3(a) show magnetization maps acquired at different stages of reversal. At 1.2 ns after the onset of the positive pulse, the image contains two dark regions at the edges, indicating that the reversal occurs through the motion of the clockwise vortex towards the top edge of the Py disk, while the counterclockwise vortex moves in from the bottom edge. A similar interpretation emerges from the analysis of the image acquired 1 ns after the onset of the negative current pulse. Almost complete chirality reversal occurs within 2 ns after the pulse onset.

Images of Fig. 3(a) provide information about the dynamical mechanism of the vortex reversal. For the uniformly

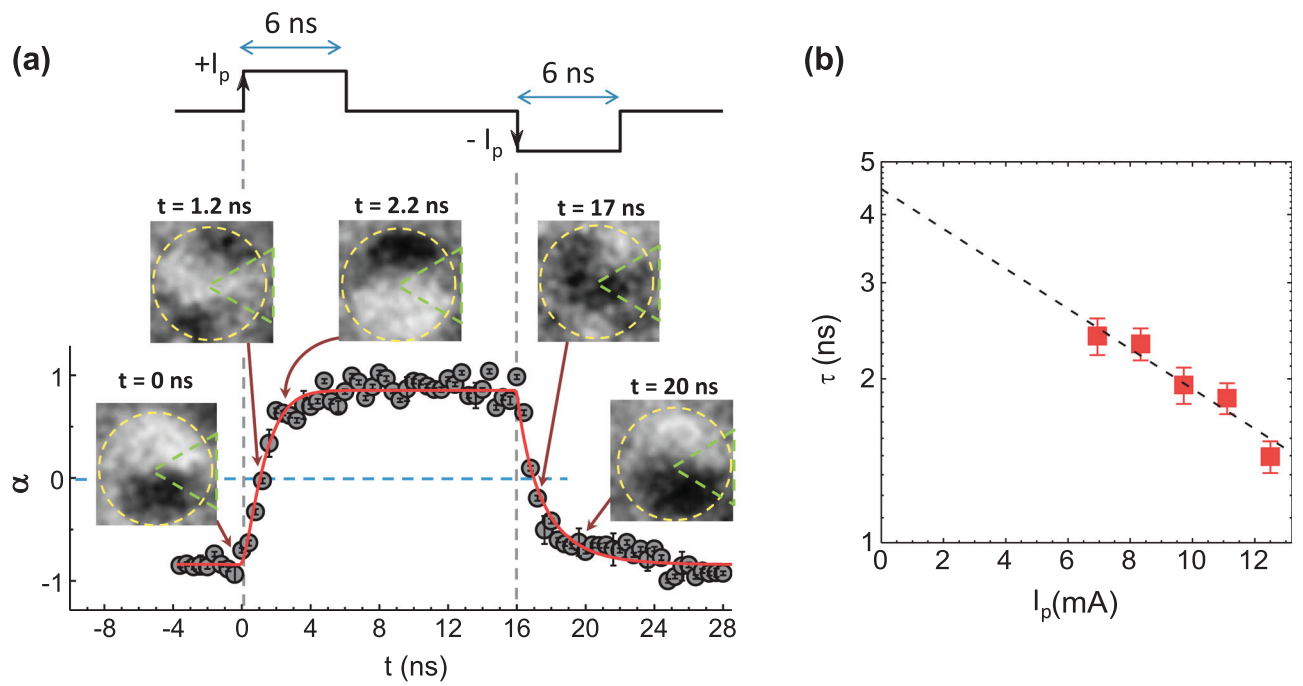

FIG. 3. Time-resolved imaging and analysis of vortex reversal. (a) Time-dependent magnetic vortex contrast obtained from the time-resolved XMCD measurements with pulsed current $I_p = \pm 12.5$ mA applied to the Pt/Py disk. The XMCD images show the initial, the intermediate, and the final states during the current pulse. The bright white (dark) corresponds to the magnetization pointing in the positive (negative) x-direction. Top panel shows the timing profile of the current pulses. The magnetic vortex state domain contrast α is defined as a spatially averaged correlation between the projected magnetization distribution of an ideal vortex and the normalized local intensity of the image. $\alpha > 0$ ($\alpha < 0$) implies an anti-clockwise (clockwise) average chirality, and $\alpha = 0$ signifies the point at which the vortex chirality, on average, switches to the opposite. Each data point (in Fig. 3(a)) is deduced from a single XMCD image. (b) Switching time vs current pulse amplitude I_P. Dashed line shows the exponential dependence that would be expected for a thermally activated process described by the Arrhenius law.

magnetized systems, the current-induced reversal is either a deterministic or a stochastic process,[27–29] depending on the driving current and the geometry of the magnetic system. In the latter case, the reversal time and the instantaneous magnetization configurations significantly vary from one reversal to another. Therefore, deterministic switching is generally more desirable for device applications. The contrast of the XMCD images acquired by averaging over many stochastic reversals would be dramatically reduced and thus, no significant redistribution of intensity would be expected at intermediate times during reversal. However, the contrasts of all the experimental images remain at similar levels, indicating that the current-induced chirality reversal in our experiment is a predominantly deterministic process.

To quantify the reversal dynamics, we calculated the effective magnetic vortex contrast α of the XMCD images (see supplementary material[30]). The time dependence of α, Fig. 3(a), indicates that reversal completes in about 2 ns after the onset of the pulse, confirming our qualitative analysis of XMCD images. We determine the average characteristic switching time $\langle\tau\rangle$ by fitting the time-dependent α with a Weibull probability distribution function (see supplementary material[30]), as shown by a red solid curve in Fig. 3(a). In different measurements at current pulse amplitudes between 6.9 mA and 12.5 mA, $\langle\tau\rangle$ approximately exponentially decreased with increasing pulse amplitude, reaching 1.4 ns at 12.5 mA (Fig. 3(b)). This dependence provides additional evidence for the deterministic vortex reversal. If we were to assume a stochastic reversal governed by the Arrhenius law, $\tau(I) = \tau_0 \exp[U_o(I)/k_BT]$, where k_B is the Boltzmann constant, T is temperature, and $U_o(I)$ is the effective current-dependent activation barrier,[31] the exponential dependence of the reversal time on the pulse amplitude would extrapolate to $\tau_0 \exp(U_o(0)) = 4.4$ ns, where $U_o(0)$ is activation barrier at $I = 0$. In contrast, in our measurements, the vortex remained stable at $I = 0$ over the duration of several hours, indicating a superexponential dependence at small currents consistent with the deterministic behaviors. Thus, the observed current dependence does not follow the exponential form of the Arrhenius law expected for thermal activation.

To gain insight into the mechanisms of vortex reversal, we performed micromagnetic simulations of current-induced magnetization dynamics using the simulation package MicroMagus[32,33] (see supplementary material[30] for details). To quantify our simulation results, we introduce the average time-dependent chirality $\langle c(t)\rangle$ defined as the normalized spatial average of the projection of the magnetization on that of the ideal counterclockwise vortex. The calculation that includes only the effects of the Oersted field shows two distinct reversal stages, Fig. 4(a). In the first stage that lasts up to 1 ns after the onset of the pulse, the chirality $\langle c(t)\rangle$ varies from -1 to 0. At the end of this stage, a highly inhomogeneous magnetization state emerges with multiple domain boundaries and a strongly distorted vortex (see inset map P1). The second stage lasts almost ten times longer, up to 10 ns after the pulse onset. During this stage, the domain boundaries gradually move out and a reversed vortex state slowly emerges after 7 ns from the upper right edge of the disk (maps P2 and P3). These results demonstrate that the effect of current-induced Oersted field alone is sufficient to reverse

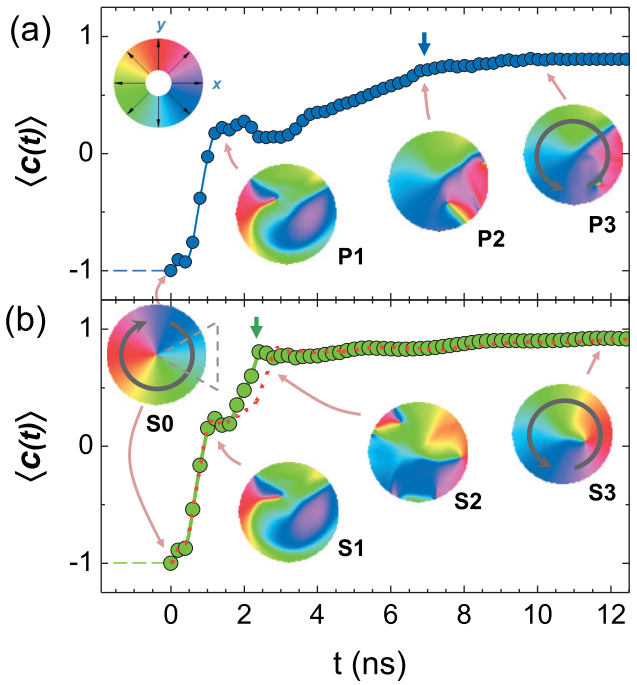

FIG. 4. Micromagnetic simulations of the current-induced vortex reversal. (a) Average chirality $\langle c(t)\rangle$ vs time t during the reversal by a pulse of current $I_p(0 < t < 6\,\text{ns}) = 13$ mA, determined in the presence of only the Oersted field, at $T = 0$ K. (b) $\langle c(t)\rangle$ vs t in the presence of both the Oersted field and the spin current, at $T = 0$ K (symbols) and $T = 300$ K (dotted red line). The insets P1–P3 and S0–S3 show the maps of the magnetization **M** in the Py disk during different stages of the vortex reversal, at $T = 0$ K. The initial state at $t = 0$ ns has a clockwise chirality ($\langle c(t)\rangle = -1$), as shown in the map S0. The points of almost complete switching ($\langle c(t)\rangle > 0.9$) at $t = 7$ ns and 2 ns in (a) and (b), respectively, are indicated by short vertical arrows. The correspondence between the in-plane direction of the magnetization and the pseudo-color is indicated on the color wheel.

the vortex chirality, but the calculated reversal time is significantly longer than experimentally observed, as shown in Fig. 3. We note that the spatial asymmetry of the reversal process is driven by the asymmetric distribution of the Oersted field, which is the largest under the pointed electrode (see supplementary material[30]).

By including the effect of ST, the second stage of the reversal process is significantly shortened, Fig. 4(b). $\langle c(t)\rangle$ increases almost up to its asymptotic value only 2 ns after the onset of the current pulse, in agreement with the experiment. Moreover, the map S2 of the magnetization during the second stage shows that the reversed vortex-like state has already formed at 2 ns, although the remnants of the original vortex are still observed near the left edge of the disk. We note that the domain boundaries in the map S2 are much shorter than in the map P2 and do not extend to the edges of the disk. These results indicate that spin transfer accelerates the formation of the reversed vortex state by efficiently overcoming the domain wall energy. The map S2 is also consistent with the experimental contrast maps, indicating that both the original and the reversed vortices are present in the disk during the intermediate stages of reversal (Fig. 3(a)). Including the effects of thermal fluctuations in addition to the Oersted field and ST resulted only in a small modification of the calculated time dependencies (dotted curve in Fig. 4(b)). Therefore, the reversal is dominated by the deterministic dynamical processes driven by a combination of the Oersted field and ST.

We have demonstrated fast deterministic current-induced reversal and electronic detection of the magnetic vortex chirality in a simple planar structure based on a bilayer of a single magnetic disk and spin Hall material Pt. The reversal is facilitated by the Oersted field of the current, while the contribution of spin transfer effect due to the spin Hall effect in Pt significantly increases the reversal speed. These results can provide a route for the development of magnetoelectronic devices utilizing inhomogeneous magnetization configurations and simultaneously take advantage of the Oersted field and the spin Hall effect. In particular, by downsizing the simple asymmetric planar geometry of our devices to nanoscale, the local radial current density and consequently both the Oersted field and the spin Hall effect can be significantly increased, enabling fast and efficient control of nanoscale inhomogeneous magnetization states such as skyrmions.

We acknowledge support from the U.S. National Science Foundation of USA and the Advanced Light Source at the Lawrence Berkeley National Laboratory.

[1]C. Chappert, A. Fert, and F. Nguyen Van Dau, Nat. Mater. **6**, 813 (2007).
[2]K. Lee and S. H. Kang, IEEE Trans. Magn. **47**, 131 (2011).
[3]L. Berger, Phys. Rev. B **54**, 9353 (1996).
[4]J. C. Slonczewski, J. Magn. Magn. Mater. **159**, L1 (1996).
[5]A. V. Khvalkovskiy, J. Grollier, N. Locatelli, Y. V. Gorbunov, K. A. Zvezdin, and V. Cros, Appl. Phys. Lett. **96**, 212507 (2010).
[6]E. B. Myers, D. C. Ralph, J. A. Katine, R. N. Louie, and R. A. Buhrman, Science **285**, 867 (1999).
[7]M. Tsoi, A. G. M. Jansen, J. Bass, W.-C. Chiang, V. Tsoi, and P. Wyder, Nature **406**, 46 (2000).
[8]S. Urazhdin, N. O. Birge, W. P. Pratt, Jr., and J. Bass, Phys. Rev. Lett. **91**, 146803 (2003).
[9]S. S. P. Parkin, M. Hayashi, and L. Thomas, Science **320**, 190 (2008).
[10]N. Nagaosa and Y. Tokura, Nat. Nanotechnol. **8**, 899 (2013).
[11]T. Shinjo, T. Okuno, R. Hassdorf, K. Shigeto, and T. Ono, Science **289**, 930 (2000).
[12]S. B. Choe, Y. Acremann, A. Scholl, A. Bauer, A. Doran, J. Stöhr, and H. A. Padmore, Science **304**, 420 (2004).
[13]B. Van Waeyenberge, A. Puzic, H. Stoll, K. W. Chou, T. Tyliszczak, R. Hertel, M. Fähnle, H. Brück, K. Rott, G. Reiss, I. Neudecker, D. Weiss, C. H. Back, and G. Schütz, Nature **444**, 461–464 (2006).
[14]V. S. Pribiag, I. N. Krivorotov, G. D. Fuchs, P. M. Braganca, O. Ozatay, J. C. Sankey, D. C. Ralph, and R. A. Buhrman, Nat. Phys. **3**, 498–503 (2007).
[15]K. Yamada, S. Kasai, Y. Nakatani, K. Kobayashi, H. Kohno, A. Thiaville, and T. Ono, Nat. Mater. **6**, 270 (2007).
[16]V. Uhlíř, M. Urbánek, L. Hladk, J. Spousta, M.-Y. Im, P. Fischer, N. Eibagi, J. J. Kan, E. E. Fullerton, and T. Šikola, Nat. Nanotechnol. **8**, 341 (2013).
[17]K. Nakano, K. Tanabe, R. Hiramatsu, D. Chiba, N. Ohshima, S. Kasai, T. Sato, Y. Nakatani, K. Sekiguchi, K. Kobayashi, and T. Ono, Appl. Phys. Lett. **102**, 072405 (2013).
[18]A. V. Khvalkovskiy, V. Cros, D. Apalkov, V. Nikitin, M. Krounbi, K. A. Zvezdin, A. Anane, J. Grollier, and A. Fert, Phys. Rev. B **87**, 020402(R) (2013).
[19]O. V. Sukhostavets, B. Pigeau, S. Sangiao, G. de Loubens, V. V. Naletov, O. Klein, K. Mitsuzuka, S. Andrieu, F. Montaigne, and K. Y. Guslienko, Phys. Rev. Lett. **111**, 247601 (2013).
[20]K. Xie, W. Lin, P. Zhang, and H. Sang, Appl. Phys. Lett. **105**, 102402 (2014).
[21]S. Urazhdin, C. L. Chien, K. Y. Guslienko, and L. Novozhilova, Phys. Rev. B **73**, 054416 (2006).
[22]L. Liu, T. Moriyama, D. C. Ralph, and R. A. Buhrman, Phys. Rev. Lett. **106**, 036601 (2011).
[23]T. Kimura, Y. Otani, T. Sato, S. Takahashi, and S. Maekawa, Phys. Rev. Lett. **98**, 156601 (2007).
[24]The device structure involves only a single magnetic layer, much simpler than that of the multilayer nanopillars. The disadvantages include the difficulty of downscaling the lateral structure and the more limited magnetoelectronic detection methods.
[25]J. Stöhr, J. Magn. Magn. Mater. **200**, 470 (1999).
[26]Y. Acremann, V. Chembrolu, J. P. Strachan, T. Tyliszczak, and J. Stöhr, Rev. Sci. Instrum. **78**, 014702 (2007).
[27]T. Devolder, J. Hayakawa, K. Ito, H. Takahashi, S. Ikeda, P. Crozat, N. Zerounian, J.-V. Kim, C. Chappert, and H. Ohno, Phys. Rev. Lett. **100**, 057206 (2008).
[28]V. Chembrolu, J. P. Strachan, X. W. Yu, A. A. Tulapurkar, T. Tyliszczak, J. A. Katine, M. J. Carey, J. Stöhr, and Y. Acremann, Phys. Rev. B **80**, 024417 (2009).
[29]I. N. Krivorotov, N. C. Emley, A. G. F. Garcia, J. C. Sankey, S. I. Kiselev, D. C. Ralph, and R. A. Buhrman, Phys. Rev. Lett. **93**, 166603 (2004).
[30]See supplementary material at http://dx.doi.org/10.1063/1.4902997 for more details on the sample fabrication, magnetoelectronic measurements, time-resolved x-ray imaging technique and analysis, calculation of the current distribution and Oersted field, and micromagnetic simulations.
[31]Z. Li and S. Zhang, Phys. Rev. B **69**, 134416 (2004).
[32]D. V. Berkov and J. Miltat, J. Magn. Magn. Mater. **320**, 1238 (2008); D. V. Berkov and N. L. Gorn, MicroMagus package for micromagnetic simulations, see http://www.micromagus.de.
[33]D. V. Berkov, "Magnetization dynamics including thermal fluctuations," in *Handbook of Magnetism and Advanced Magnetic Materials*, Micromagnetism Vol. 2, edited by H. Kronmüller and S. Parkin (John Wiley & Sons, Ltd., Chichester, UK, 2007), p. 795.